Journal of Power Sources 196 (2011) 2149–2154

Contents lists available at ScienceDirect

Journal of Power Sources

journal homepage: www.elsevier.com/locate/jpowsour

# Vanadium-substituted porous manganese oxides with Li-ion intercalation properties

M.K. Gulbinska [a,*], S.L. Suib [b]

[a] Yardney Technical Products, Inc., 82 Mechanic Street, Pawcatuck, CT 06379, USA
[b] Department of Chemistry, Unit 3060, University of Connecticut, Storrs, CT 06269, USA

ARTICLE INFO

*Article history:*
Received 17 August 2010
Received in revised form 1 October 2010
Accepted 4 October 2010
Available online 8 October 2010

*Keywords:*
Lithium-ion
Cathode
Materials
Intercalation
Potential

ABSTRACT

In this study, vanadium ions were substituted for manganese in the crystal lattice of synthetic cryptomelane, also denoted as OMS-2, via microwave field-assisted syntheses. Doping vanadium into the framework of mixed valence manganese oxide resulted in OMS-2 materials with modified composition, morphology, and electrical properties. Structural properties and morphology of synthesized materials were characterized by XRD and FESEM, respectively. Average oxidation state and resistivity measurements were also taken. The effect of framework doping of vanadium ions on lithium-ion intercalation properties of manganese oxides was investigated in Li-ion cathode half-cells.



## 1. Introduction

Synthetic cryptomelane ($KMn_8O_{16}\cdot nH_2O$), also called OMS-2, is a potassium form of the manganese oxide mineral, hollandite. OMS-2 belongs to a unique class of synthetic porous manganese oxides, denoted as octahedral molecular sieves, OMS [1–3]. These porous manganese oxides exhibit one-dimensional arrangements of tunnels, formed by the edge- and corner-shared $MnO_6$ coordination octahedral [4]. In the OMS-2 structure, the double chains of edge-sharing $MnO_6$ octahedra share corners and form the square $(2 \times 2)$ tunnel openings with the 4.6 Å by 4.6 Å dimensions. The tetragonal unit cell of cryptomelane has $a = 9.84$ Å, and $c = 2.85$ Å parameters, as described by Ramsdell [5].

One of the unique properties of the OMS-type materials is the presence of both, $Mn^{3+}$ and $Mn^{4+}$ ions in the manganese oxide framework. Thus, the average oxidation state of manganese in the OMS-type materials ranges from 3.4 to 3.99, depending on the $Mn^{4+}/Mn^{3+}$ ratio. For the vanadium-free cryptomelane later referred to as K-OMS-2, the average oxidation state of manganese equals to 3.9 varying slightly with the applied synthesis method. Materials with similar overall compositions and structures may perform very differently either as catalysts or electrochemically active materials, depending on their syntheses conditions. These differences in performance may be attributed to variations in particle size and the type and amount of defects present in the crystal structures [2].

In the previous studies, porous manganese oxide materials have been prepared via a variety of routes [6–8]. In this study, hydrothermal syntheses were performed in a microwave field. Irradiation with the microwave energy has generated much interest as a possible heating method yielding nano-sized particles [9,10]. When irradiated with microwaves, the bulk of the material directly absorbs the energy. Thus, uniform and rapid heating may be achieved quickly through microwave irradiation. Values of dielectric constants and dielectric loss factors of materials furnish information about the strength of the interactions of the electromagnetic field with molecules of the heated substance. Since the dielectric constants for manganese oxides are very large (as high as 105), microwave irradiation has a tremendous effect on the syntheses of porous manganese oxides [11,12].

Post-synthetic alterations of the porous manganese oxides, such as the ion exchange, have also been explored [13–15]. Previous work has mostly been focused on the doping of different divalent metal cations into the tunnels of OMS-2 [16]. Very few studies have attempted the incorporation of transition metal cations into the framework of OMS-2 [1,17]. Notably, Polverejan et al. [1] prepared vanadium-doped OMS-2 materials by a conventional hydrothermal synthesis method. In this work, microwave-assisted heating was used and the synthetic method of choice affected the properties of the as-obtained manganese oxides, such as vanadium contents, and the morphology of OMS-2 material.

* Corresponding author. Tel.: +1 118605991100; fax: +1 118605995122.
*E-mail addresses:* mgulbinska@lithion.com, mgulbinska@gmail.com (M.K. Gulbinska).

0378-7753/$ – see front matter © 2010 Elsevier B.V. All rights reserved.
doi:10.1016/j.jpowsour.2010.10.010

The mixed valence properties of the OMS materials and the presence of tunnels in their crystal structures have prompted much research interest and many attempts at various applications of this class of materials [2,18] The catalytic applications in oxidation/reduction reactions of organic and inorganic compounds remain among the most prominent uses [19,20]. However, electrochemical applications of OMS-type materials have also received interest [2]. Structural and electrochemical studies of α-$MnO_2$ (dehydrated cryptomelane), stabilized with $Li_2O$ present in the tunnels instead of the $K^+$ ions and $H_2O$ were performed by Johnson et al. [21,22]. Pistoia and Antonini described the electrochemical behavior of selected polymorphs of $MnO_2$, such as α-, β-, γ-$MnO_2$ [23]. Ohzuku et al. investigated the effects of various stabilizing cations ($K^+$, $NH_4^+$, and $Rb^+$) on $Li^+$ intercalation within the $2 \times 2$ tunnels of α-$MnO_2$ [24]. To the best of the authors' knowledge, the effect of high-valency ion substitution into the OMS-type structures and derivatives on their lithium-ion intercalation properties was not yet studied. In this work, we report the electrochemical discharge results for the $V^{5+}$-doped OMS-2 materials with varying vanadium contents. The effect of $V^{5+}$-doping on the structure, particle size, average oxidation state, and resistivity of the OMS-2 materials is also discussed.

## 2. Experimental

### 2.1. Microwave-assisted syntheses

A microwave oven (Milestone, Ethos Pro™) was utilized in the microwave field-assisted syntheses. The reaction temperature was measured *in situ* with an insulated thermocouple inserted into the reference vessel. Microwave-heated materials were synthesized at 200 °C for 24 h. A typical synthesis of vanadium-substituted OMS-2 material, K-V-OMS-2, involves the microwave field irradiation of a 50-mL aqueous suspension of 11.9 mmol $MnSO_4 \cdot H_2O$, $K_2S_2O_8$, and $K_2SO_4$ in a molar ratio of 2:3:3. Sodium ortho-vanadate was added such that the Mn/V molar ratio was 9 and 19 for the materials with 5% and 10% of vanadium contents, respectively. The entire mixture was autoclaved at 200 °C in a microwave oven for 24 h. The product was filtered, washed with deionized water, and dried at 110 °C overnight.

### 2.2. Elemental composition

The energy dispersive spectra were obtained at the Connecticut College, using the LEO 435VP scanning electron microscope, equipped with an EDX detector.

### 2.3. Average oxidation state of manganese

A potentiometric titration was used to measure the average oxidation state of manganese in all synthesized samples. The two-step procedure involved determination of the total Mn content in manganese oxide samples, followed by the measurement of available oxygen. The complete potentiometric titration procedure has been described previously [25].

### 2.4. Structural characterization

X-ray diffraction patterns of the coatings were obtained with a Scintag X-ray diffractometer model XDS-2000 equipped with a CuKα radiation source with a beam voltage of 45 kV and a 40-mA beam current. Powders were placed onto an aluminum sample holder and pressed flat. The scan angle was set at 5–65° with a 1° $min^{-1}$ rate of analysis. The Rietveld refinement of lattice parameters based on XRD data was performed using the General Structure Analysis System (GSAS) [26].

**Table 1**
Elemental analyses and average oxidation state titration results.

| Sample | Initial | EDX ± 0.2 | | | AOS ± 0.3 |
|---|---|---|---|---|---|
| | % V | K [%] | V [%] | Mn [%] | |
| K-V-OMS-2(6.3) | 10 | 11.2 | 6.3 | 82.5 | 3.58 |
| K-V-OMS-2(3.5) | 5 | 11.9 | 3.5 | 84.6 | 3.76 |
| K-OMS-2 | 0 | 11.9 | 0 | 88.1 | 3.91 |
| K-OMS-2(HT)[a] | 0 | 8.5 | 0 | 91.5 | 3.87 |

[a] K-OMS-2(HT) sample was synthesized via hydrothermal methods.

### 2.5. Morphology

A Zeiss EM910 120 keV high-resolution scanning electron microscope was used to examine the surface morphologies of all materials.

### 2.6. DC electrical resistivity measurements

Samples of K-OMS and K-V-OMS-2 weighing about 0.3 g were pressed into approximately 1-mm thick discs, with the 13-mm diameters using an applied pressure of about 10,000 pounds for 3 min. Glass slides were used as sample holders. The discs were secured to the glass slides by using a non-conductive epoxy resin. Platinum wires were then attached to the discs using a conductive silver paint. Details of this procedure are described elsewhere [27].

### 2.7. Coin half-cell assembly and cycling

The electrochemical performance of the synthesized materials was evaluated in cathode coin half-cells. Cathode solids including: 30 wt.% of Kynarflex 2801 binder (Atofina Chemicals, Inc.), 5 wt.% KS-15 graphite (Timcal), 5 wt.% Super P carbon (Comilog, S. A.) and 60 wt.% of active material (OMS-2), were dispersed in the n-methyl-2-pyrrolidone solvent (Brand-Nu Laboratories, Inc.). The weight ratio of solids to solvent was 1:1. The resulting slurry was stirred and sonicated for 30 min, and then spread onto the aluminum foil current collector. Coated foils were placed in a vacuum oven at 110 °C for 12 h. The cathode coin half-cells, containing metallic lithium as the anode, were assembled under argon atmosphere inside a glove box. Coin cells contained an electrolyte solution of 1.0 M $LiPF_6$ dissolved in a 1/1/1 (v/v/v) EC/DMC/DEC mixture. The cells were cycled at room temperature with 0.38 mA $cm^{-2}$ current density in order to determine the cell voltage, capacity, and the discharge cycling efficiency of the cathode.

## 3. Results

### 3.1. Elemental analyses

EDX analyses were performed in order to establish manganese, vanadium and potassium contents in OMS-2 samples (Table 1). The structure favored a higher Mn/V ratio than the one initially present in the reaction mixture prior to crystallization. EDX results show increased vanadium content with higher V/Mn ratio, accompanied by a decrease in the amount of framework manganese, and about constant potassium percentage. Polverejan et al. [1] contributed the changes in contents of Mn and V to isomorphous substitution of $V^{5+}$ for $Mn^{4+}$ rather than replacement of $K^+$ ions in the tunnels.

### 3.2. Average oxidation state

Vanadium doping caused a decrease in the average oxidation state (AOS) of manganese (Table 1). The mixed valency of the undoped K-OMS-2 sample is manifested in the AOS value of 3.9, with both $Mn^{3+}$ and $Mn^{4+}$ present in the manganese oxide framework.

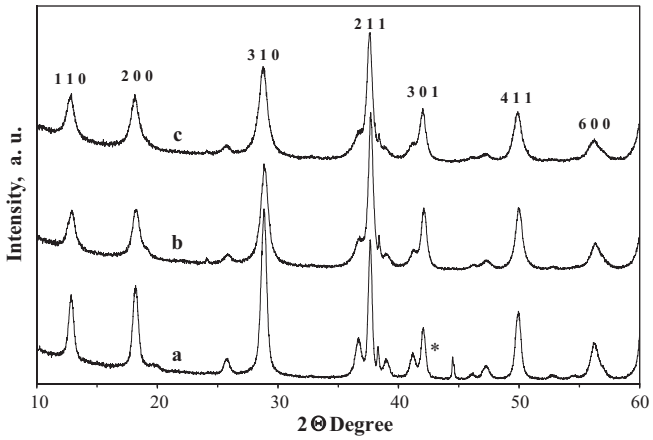


**Fig. 1.** XRD patterns of K-V-OMS-2 materials synthesized in a microwave field. Miller indices ($h\,k\,l$) are shown above the top pattern. The bottom X-ray pattern (a) corresponds to the vanadium-free K-OMS-2 material. The marker (*) over the diffraction pattern (a) denotes the peak intensity from an aluminum sample holder. The middle X-ray pattern (b) represents the K-V-OMS-2(3.5) material with the nominal 3.5% V. The K-V-OMS-2(6.3) sample with 6.3% V is shown in pattern (c).

The contribution of $Mn^{4+}$ ions gradually decreased with increasing vanadium content, leading to the lowest manganese AOS value of 3.56 for the K-V-OMS-2 sample with 6.3% vanadium content.

### 3.3. XRD

X-ray powder diffraction results for synthesized samples are shown in Fig. 1. The bottom XRD pattern (a) represents the non-substituted K-OMS-2 sample. X-Ray diffraction patterns (b) and (c) correspond to the K-V-OMS-2 materials with the vanadium contents of 3.5% and 6.3%, respectively. The XRD pattern for non-substituted K-OMS-2 material exhibits greater crystallinity, manifested as relatively intense and narrow XRD peaks, compared to broad peaks observed in (b) and (c) patterns. The XRD pattern for K-OMS-2 sample (a) exhibits preferred orientations, but the peak intensities observed in (b) and (c) patterns remain relatively unaffected. The absence of preferred orientations in substituted samples is consistent with the morphology data (Figs. 2 and 3) that will be described more closely in the discussion section.

**Table 2**
GSAS lattice parameter refinement results (26) for K-OMS-2 sample synthesized in a microwave field.[a]

| Sample | Unit cell parameters (Å) | | Profile parameters | | |
|---|---|---|---|---|---|
| | $a \pm 0.0006$ | $c \pm 0.0003$ | Volume (Å$^3$) | $\chi^2$ | $R(F^2)$ [%] |
| K-OMS-2 | 9.8452 | | 277.414 | 5.070 | 8.37 |

[a] Space group: I4/m, $\alpha = \beta = \gamma = 90^\circ$.

Experimental d-spacings (Å) observed in X-ray diffraction patterns of synthesized OMS-2 samples (Fig. 1) coincide with those found in JCPDS card number 29-1020 for synthetic cryptomelane-Q. No additional peaks, corresponding to crystalline vanadium oxides, were observed.

Crystal lattice parameter refinement results and profile parameters for K-OMS-2 data are shown in Table 2. The refined unit cell parameters (Table 2) are consistent with $a = 9.84$ Å, and $c = 2.85$ Å values described by Ramsdell [5] Corresponding XRD data for vanadium-substituted materials were not refined due to inherently broad XRD peaks observed in the nano-particulate K-V-OMS-2 samples.

### 3.4. Morphology

High-resolution electron micrographs in Fig. 2a and b show the needle-like particles of non-substituted K-OMS-2 material. Individual particles of OMS-2 are well developed, and there is no visual indication of additional phases with different morphology. Bundles and individual needles of the K-OMS-2 material exceed 2 μm in length. Much shorter particles are formed during syntheses of vanadium-substituted samples. About 200-μm particles, shown in Fig. 3a, belong to the vanadium-substituted manganese oxide

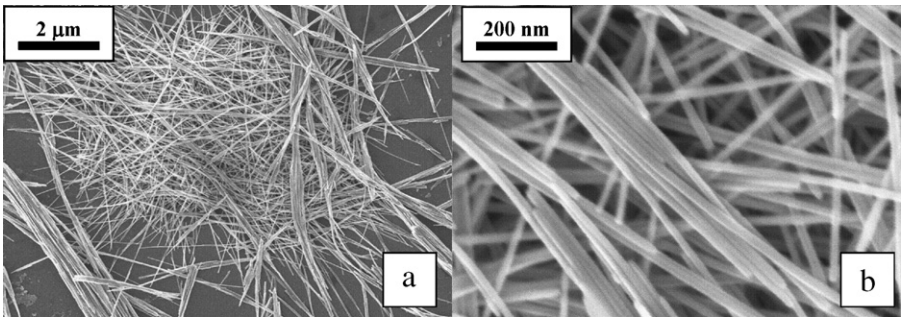


**Fig. 2.** High-resolution electron micrographs of the K-OMS-2 material synthesized in a microwave field, taken at two different magnifications.

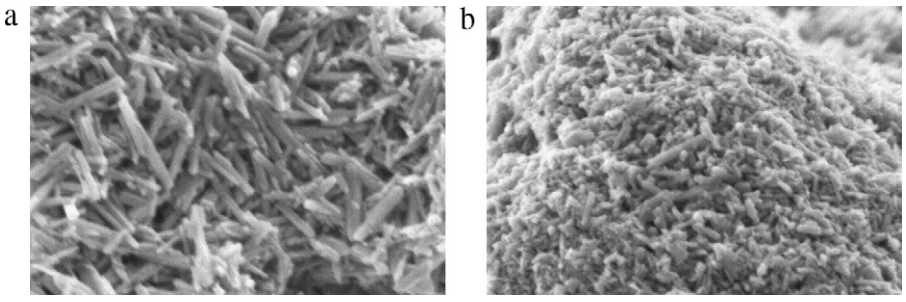


**Fig. 3.** High-resolution electron micrograph of the K-V-OMS-2 materials synthesized in a microwave field. Micrograph (a) corresponds to the K-V-OMS-2(3.5) material with 3.5% V. Micrograph (b) illustrates the K-V-OMS-2(6.3) sample with 6.3% V.

**Table 3**
Resistivity ($\rho$) and conductivity ($\sigma$) values of samples with varying vanadium contents.

| Sample | $\rho$ ($\Omega$ cm) [$\times 10^2$] | $\sigma$ ($\Omega$ cm$^{-1}$) [$\times 10^{-2}$] |
|---|---|---|
| K-V-OMS-2 10% V | 7.9 | 0.13 |
| K-V-OMS-2 5% V | 6.9 | 0.15 |
| K-OMS-2 | 0.14 | 7.1 |
| Ref.: K-OMS-2(HT) | 0.49 | 2.1 |

with 3.5% vanadium content. The reaction mixture with a nominal 10% vanadium concentration yields a product with the actual 6.3% V content and with <100 μm-long particles (Fig. 3b). Needle-like particles in all vanadium-substituted manganese oxides are short but well developed and there is no visible evidence of particles with other morphology. The small size-aspect ratio in substituted OMS-2 materials causes less pronounced preferred orientations in X-ray diffraction patterns of these materials when compared to non-substituted samples.

### 3.5. Resistivity

The room temperature DC resistivities were measured for the K-OMS-2 and K-V-OMS-2 materials by four-probe method, with a current of 0.1 mA. The resistivity values for K-OMS-2 and K-V-OMS-2 materials are listed in Table 3. Insertion of vanadium-ions into the mixed-valency manganese oxide frameworks causes an increase in resistivity of the doped materials because of the formation of traps on the $V^{5+}$ sites and the resulting interruption in electron hopping between $Mn^{3+}$ and $Mn^{4+}$ [27].

### 3.6. Coin cell cycling results

The Li/OMS-2 cells were cycled galvanostatically with the 0.38 mA cm$^{-2}$ current density. The first discharge and charge curves for OMS-2 materials are shown in Fig. 4. Curve (a) corresponds to the un-exchanged OMS-2 material. For clarity, the capacity derivative was plotted against voltage in Fig. 5. The cycling behavior of the OMS-2 materials undergoes changes upon vanadium ion incorporation into the manganese oxide framework. Vanadium-substituted materials have flatter discharge profiles (Fig. 4b and c), compared to the sloping curve for vanadium-free manganese oxide illustrated in Fig. 4a. In a capacity derivative plot (Fig. 5), the multiple peaks observed in K-OMS-2 material (a) collapse into one peak with a shoulder at about 2.6 V observed in both $V^{5+}$-doped samples.

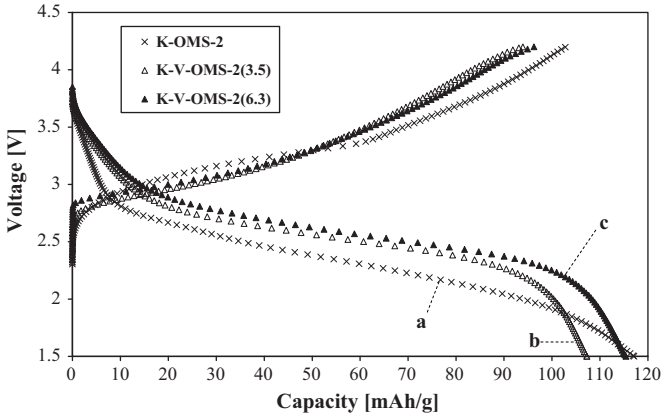


**Fig. 4.** Coin cell cycling results for K-V-OMS materials synthesized in a microwave field. Profile (a) corresponds to the K-OMS-2 material (the vanadium-free OMS-2). Profile (b) represents the K-V-OMS-2(3.5) material with 3.5% V. Profile (c) corresponds to the K-V-OMS-2(6.3) sample with 6.3% vanadium.

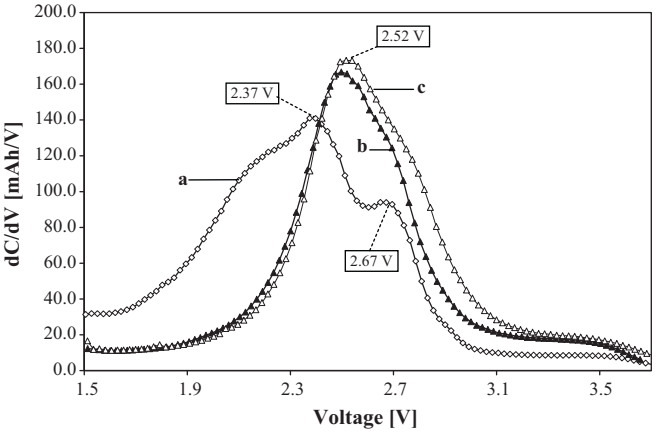


**Fig. 5.** Capacity derivative plots (d$C$/d$V$ vs. voltage) of the coin cell results for K-V-OMS materials. Plot (a) corresponds to the K-OMS-2 material (the undoped OMS-2). Plot (b) represents the K-V-OMS-2(3.5) material with 3.5% V. Plot (c) shows results for the K-V-OMS-2(6.3) sample with 6.3% vanadium.

Clearly, the lithium-ion insertion process into the K-V-OMS-2 tunnels proceeds in a topotactic manner, without the phase change throughout the entire cycling voltage range (1.5–3.8 V). The first discharge voltage values shift to higher values with the increasing vanadium content (Fig. 4). The specific capacity for first discharge in K-OMS-2 material was 117 mAh g$^{-1}$. The discharge of vanadium-doped K-V-OMS-2 materials resulted in 107 mAh g$^{-1}$ (3.5% V) and 115 mAh g$^{-1}$ (6.3% V) capacity values. With the maximum experimental deviation of ±8 mAh g$^{-1}$ for a set of three coin cells, the observed specific capacity values for K-OMS-2 and its vanadium derivatives are statistically the same. No significant capacity loss was observed upon vanadium incorporation.

## 4. Discussion

Elemental analyses results (DCP and EDX) show the gradual compositional changes in manganese and vanadium due to the isomorphous substitution of $V^{5+}$ for $Mn^{4+}$ in manganese oxide frameworks. When the amount of vanadium is increased, the manganese content steadily decreases, while the percentage of potassium counter-ion is relatively constant. The framework charge compensation via decrease in the $Mn^{4+}/Mn^{3+}$ ratio with the increasing $V^{5+}$ content was suggested in an earlier work [1]. Polverejan et al. [1] has also reported that for samples with low vanadium contents (i.e., 10% vanadium and less), the initial percentage of vanadium in the reacting mixture was close to the final product composition. The discrepancy between the starting amount of vanadium and the framework-incorporated species seems to be more pronounced in the microwave field syntheses (samples with the 10% starting vanadium show the 6.3% of incorporated vanadium by DCP analyses). The microwave-field heated materials incorporate more potassium into the OMS-2 tunnels (>11% by EDX) than their conventionally heated counterparts (~8%) while the manganese contents are comparable in the MW- and conventionally-prepared materials, respectively [1]. The work by Vileno et al. [12], described the relationship between enhanced solubility of reactants and intermediates in a microwave field and the final composition of $Mg^{2+}$-doped manganese oxides (todorokite-type OMS-1).

The average oxidation state (AOS) measurements confirm the $V^{5+}$ substitution for $Mn^{4+}$. Manganese AOS values in OMS-2 materials decrease gradually with increasing vanadium contents (Table 1). The microwave-irradiated, undoped K-OMS-21 material exhibits higher AOS value than its conventionally heated counterpart.

Vileno et al. [12] contributed the higher oxidation numbers (AON) of microwave-aged samples over the conventionally heated materials to the absence of formation or a fast dissolution of the lower oxidation state impurities, such as $Mn_3O_4$ and $Mn_2O_3$.

Structural characterizations by X-ray powder diffraction have shown that vanadium ions were uniformly incorporated into the manganese oxide frameworks, without forming crystalline impurities. No additional X-ray diffraction peaks, corresponding to crystalline vanadia phases, were found in any of the XRD patterns. All the experimental d-spacings (Å) in synthesized OMS-2 samples correspond to the *h k l* indexed planes found in synthetic cryptomelane-Q (JCPDS card number 29-1020). No evidence of change in d-spacings was found within the experimental range of vanadium concentrations (0–10% V in the reagent mixture). The similarity in ionic radii of $Mn^{4+}$ (0.53 Å) and that of $V^{5+}$ (0.54 Å) can be credited for the unchanged value of basal spacing in various K-V-OMS-2 materials [28]. Lattice parameters refinement results of the undoped manganese oxide gave the parameters $a = 9.8452$ Å and $c = 2.8620$ Å that are in agreement with those described by Ramsdell [5] for cryptomelane structure ($a = 9.84$ Å and $c = 2.85$ Å). Data for the vanadium-exchanged materials were not refined due to the progressive broadening of experimental XRD lines that was caused by the gradual decrease in particle size of K-V-OMS-2 materials with the increasing V/Mn ratios.

Further evidence of the decrease in particle size with increasing vanadium content is illustrated in Figs. 2 and 3. The high-resolution micrographs of vanadium-free K-OMS-2 material (Fig. 2) exhibit the needle-shaped particles that are more than 2 μm long and about 20 nm wide. The K-V-OMS-2(3.5) particles with 3.5% vanadium content are, on the average, shorter than 200 nm. Particles of the material with highest vanadium content (6.5% vanadium) are <100 nm long. A dramatic effect of vanadium doping on the average particle length can be related to interactions of the microwave field with the high-valency ion doped manganese oxide frameworks. Dielectric relaxation in mixed-valence manganese oxides occurs largely through electron hopping [29] between $Mn^{4+}$ and $Mn^{3+}$ ions. High-valency $V^{5+}$ ion substitution disrupts the electron movement within the OMS-2 lattice, and lowers the amount of microwave energy absorbed by growing K-V-OMS-2 crystals, thus suppressing the particle growth.

The disturbance of electron hopping, caused by $V^{5+}$-doping, also affects the conductivity of the MW-synthesized materials. Formation of the electron traps on the $V^{5+}$ sites increases the resistivity values for doped materials by an order of magnitude (Table 3). The K-V-OMS-2(6.3) material with 6.3% vanadium exhibits resistivity of $7.9 \times 10^2\ \Omega$ cm, compared to $0.14 \times 10^2\ \Omega$ cm for the microwave-irradiated vanadium-free OMS-2 material. A conventional, hydrothermal synthesis of the K-OMS-2 yields a product with a resistivity of $0.49 \times 10^2\ \Omega$ cm.

The coin cell cycling data for the first discharge indicate that the progressive $V^{5+}$-doping affects the lithium-insertion behavior of K-V-OMS-2 materials (Fig. 4). The greatest difference can be observed in first discharge curves for the vanadium-free material and its 3.5% vanadium derivative. A sloping curve for the undoped OMS-2 is comparable to the discharge behavior of the α-$MnO_2$ reported in the literature [24], whereas the V-exchanged materials possess flatter discharge profiles that shift towards higher voltages with increasing vanadium content (Fig. 4). There was no significant decrease in capacity of manganese oxide cathodes on vanadium incorporation into the OMS-frameworks. The observed increase in $Li^+$ intercalation voltage, accompanied by the apparent lack of capacity loss on vanadium incorporation can be of practical importance in attempts to increase the operating voltage of manganese oxide-based cathode materials for lithium-ion batteries.

The specific capacity value of 117 mAh $g^{-1}$ (~48% theoretical capacity) for the undoped K-OMS-2 is lower than the reported values for the dehydrated α-$MnO_2$ (>168 mAh $g^{-1}$). However, a high $K^+$ content in the MW-synthesized material is expected to hinder $Li^+$ insertion due to the electrostatic repulsion between $K^+$ and $Li^+$ ions within the $2 \times 2$ channels. The presence of stabilizing water molecules in the OMS-2-type structures is known to decrease the observed discharge capacity values. The purpose of this study was to characterize the framework-substituted materials with varying vanadium contents, with structural stability being of primary importance over achieving the maximum electrochemical performance. The chemical lithiation, and/or the complete removal of water from OMS-2 tunnels will be pursued in future work.

## 5. Conclusions

Microwave field-assisted methods were successfully applied in syntheses of the vanadium-doped manganese oxides materials with the OMS-2 structure. The $V^{5+}$ ions were substituted for $Mn^{4+}$ in the mixed valence ($Mn^{4+}/Mn^{3+}$) manganese oxide framework. The crystal structure of synthetic cryptomelane was retained in vanadium-doped materials. The average particle size, conductivity and the average oxidation state of manganese decreased gradually with the increasing vanadium content in the OMS-2 frameworks. When tested in Li-ion batteries, vanadium-doped cathode materials exhibited flat discharge profiles that shifted towards higher voltages with increasing vanadium content without significant changes in discharge capacity values.

## Acknowledgements

Authors would like to thank Dr. Katana Ngala, and Dr. Francis S. Galasso of University of Connecticut, and Doctors: Joseph F. DiCarlo, Thomas Barbarich and Boris Ravdel of Yardney, Inc. for their help and insightful comments. The authors also thank the Geosciences and Biosciences Division, Office of Basic Energy Sciences, Office of Science, US Department of Energy for financial support.

## References

[1] M. Polverejan, J.C. Villegas, S.L. Suib, J. Am. Chem. Soc. 126 (2004) 7774.
[2] S.L. Brock, N. Duan, Z.R. Tian, O. Giraldo, H. Zhou, S.L. Suib, Chem. Mater. 10 (1998) 2619.
[3] C. Laberty, S.L. Suib, A. Navrotsky, Chem. Mater. 12 (2000) 1660.
[4] G.-G. Xia, W. Tong, E.N. Tolentino, N.-G. Duan, S.L. Brock, J.-Y. Wang, S.L. Suib, Chem. Mater. 13 (2001) 1585.
[5] A. Ramsdell, Am. Mineral. 27 (1942) 611.
[6] Y.F. Shen, S.L. Suib, C.L. O'Young, J. Catal. 161 (1996) 115.
[7] H. Zhou, X.C. Wang, C.L. O'Young, S.L. Suib, J. Catal. 176 (1998) 321.
[8] T.K. Katranas, A.C. Godelitsas, A.G. Vlessidis, N.P. Evmiridis, Micropor. Mesopor. Mater. 69 (2004) 165.
[9] M. Nakayama, K. Watanabe, H. Ikuta, Y. Uchimoto, M. Wakihara, Solid State Ionics 164 (2003) 35.
[10] S.S. Manoharan, S.J. Prasanna, M.L. Rao, R.K. Sahu, J. Am. Ceram. Soc. 85 (2002) 2469.
[11] Q. Zhang, J. Luo, E. Vileno, S.L. Suib, Chem. Mater. 9 (1997) 2090.
[12] E. Vileno, H. Zhou, Q. Zhang, S.L. Suib, D.R. Corbin, T.A. Koch, J. Catal. 187 (1999) 285.
[13] S. Ching, P.F. Driscoll, K.S. Kieltyka, M.R. Marvel, S.L. Suib, Chem. Commun. 23 (2001) 2486.
[14] J. Cai, J. Liu, S.L. Suib, Chem. Mater. 14 (2002) 2071.
[15] J. Cai, S.L. Suib, Inorg. Chem. Commun. 4 (2001) 493.
[16] X. Chen, Y.-F. Shen, S.L. Suib, C.L. O'Young, Chem. Mater. 14 (2002) 940.
[17] J. Cai, J. Liu, W.S. Willis, S.L. Suib, Chem. Mater. 13 (2001) 2413.
[18] A.A. Fakhreia, I.Z. Mohamed, Micropor. Mesopor. Mater. 67 (2004) 43.
[19] J. Luo, Q. Zhang, A. Huang, O. Giraldo, S.L. Suib, Inorg. Chem. 38 (1999) 6106.
[20] E. Vileno, Y. Ma, H. Zhou, S.L. Suib, Micropor. Mesopor. Mater. 20 (1998) 3.
[21] C.S. Johnson, D.W. Dees, M.F. Mansuetto, M.M. Thackeray, D.R. Vissers, D. Argyriou, C.-K. Loong, L. Christensen, J. Power Sources 68 (1997) 570.
[22] C.S. Johnson, M.F. Mansuetto, M.M. Thackeray, Y. Shao-Horn, S.A. Hackney, J. Electrochem. Soc. 144 (1997) 2279.
[23] G. Pistoia, A. Antonini, J. Electrochem. Soc. 144 (1997) 1553.

[24] T. Ohzuku, M. Kitagawa, K. Sawai, T. Hirai, J. Electrochem. Soc. 138 (1991) 360.
[25] D. Glover, B. Schumm, A. Kazowa, Handbook of Manganese Dioxides Battery Guide, Int. Battery Mater. Assoc., 1989.
[26] A.C. Larson, R.B. Von Dreele, General Structure Analysis System (GSAS), 2000, Los Alamos National Laboratory Report LAUR, 86-748.
[27] R.N. De Guzman, A. Awaluddin, Y.-F. Shen, Z.R. Tian, S.L. Suib, S. Ching, C.-L. O'Young, Chem. Mater. 7 (1995) 1286.
[28] D.R. Lide, CRC Handbook of Chemistry and Physics, 82nd ed., CRC Press, Boca Raton, FL, 2001, pp. 12–15.
[29] A.K. Jonscher, J. Phys. D: Appl. Phys. 32 (1999) R57.